CHEMISTRY OF MATERIALS

Article

pubs.acs.org/cm

# Thiophene Fused Azacoronenes: Regioselective Synthesis, Self-Organization, Charge Transport and Its Incorporation in Conjugated Polymers

Bo He,[†,⊥] Andrew B. Pun,[†,⊥] Liana M. Klivansky,[†] Alexandra M. McGough,[†] Yifan Ye,[‡,§] Junfa Zhu,[‡,§] Jinghua Guo,[‡] Simon J. Teat,[‡] and Yi Liu*[,†]

[†]The Molecular Foundry and [‡]Advanced Light Source, Lawrence Berkeley National Laboratory, One Cyclotron Road, Berkeley, California 94720, United States

[§]National Synchrotron Radiation Laboratory, University of Science and Technology of China, Hefei 230029, China

Supporting Information

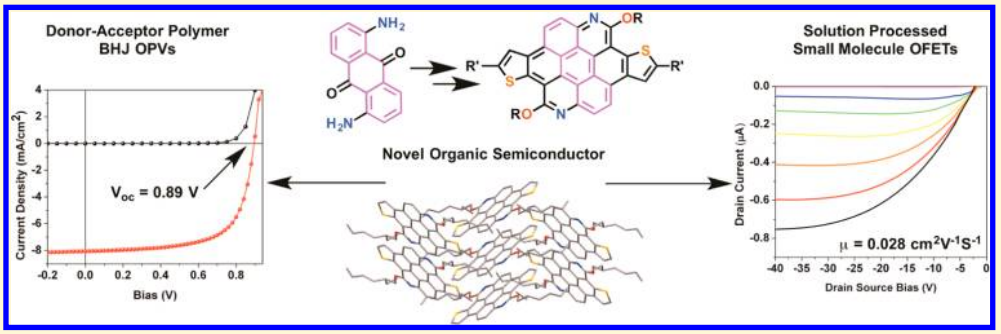


**ABSTRACT:** A regioselective synthesis of an azacoronene fused with two peripheral thiophene groups has been realized through a concise synthetic route. The resulting thienoazacoronene (TAC) derivatives show high degree of self-organization in solution, in single crystals, in the bulk, and in spuncast thin films. Spuncast thin film field-effect transistors of the TACs exhibited mobilities up to 0.028 $cm^2\ V^{-1}\ S^{-1}$, which is among the top field effect mobilities for solution processed discotic materials. Organic photovoltaic devices using TAC-containing conjugated polymers as the donor material exhibited a high open-circuit voltage of 0.89 V, which was ascribable to TAC's low-lying highest occupied molecular orbital energy level.

## INTRODUCTION

Organic semiconductors with controllable molecular packing have great potential for use in high performance electronic devices,[1] such as organic field effect transistors (OFETs)[2] and organic photovoltaics (OPVs).[3] Polycyclic aromatic hydrocarbons (PAHs)[4] and heterocyclic PAHs that contain N,[5] S[6] and O[7] heteroatoms in their aromatic skeletons have a strong propensity to stack into one-dimensional (1D) columns that serve as the preferred charge transport pathway.[8] Thiophene-fused heterocyclic PAHs have received increasing attention because they combine the unique electronic structure of the smallest benzenoid graphene and the excellent electronic properties of thiophene.[9] Recently, several groups have reported multithiophene-annulated coronene systems (Scheme 1),[10] particularly the hexathienocoronenes (HTC)[10d,f] and contorted dibenzotetrathienocoronenes (DBTTC)[10b,c,e] that have shown great self-assembly behavior and promising electronic properties. To incorporate these thienocoronenes into functional molecular frameworks such as polymers, it is desirable to have a bisthienocoronene system that can give rise to difunctional monomers. Despite the reported synthesis of electron deficient dithienocoronene diimide (DTCDI) from perylene diimide precursors,[11] efficient synthesis of such molecular systems that gives high yield and regioselectivity still remains a very challenging task. Here we present a rapid and large-quantity synthesis of a thienoazacoronene (TAC) unit that features two fused thiophenes and two N atoms on the core, and two peripheral alkoxyl groups (Scheme 1). As shown by single crystal X-ray analysis, grazing incidence wide-angle X-ray scattering (GIWAXS), and angular dependent near-edge X-ray absorption fine structure spectroscopy (ADNEXAFS), the TACs have excellent self-organization proper-

**Scheme 1. Multi-Thiophene-Fused Coronene Systems**

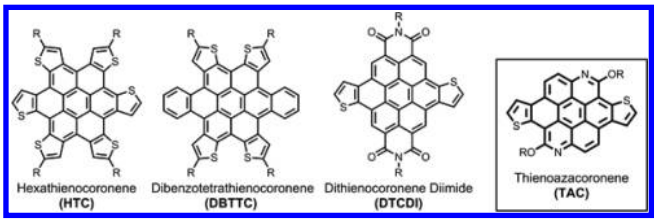


Received: April 17, 2014
Revised: June 12, 2014
Published: June 14, 2014

 © 2014 American Chemical Society 

ties, which corroborate with good field effect mobilities in spuncast films. OPV devices using a TAC-containing conjugated polymer as the donor material have a high open circuit voltage of 0.89 V, suggesting that TAC is a valuable, low highest occupied molecular orbital (HOMO) electron donor for tuning the energy levels in hole transporting polymers.

## EXPERIMENTAL SECTION

**Materials Synthesis.** The synthetic route is outlined in Scheme 2. Compound **1** was purchased from Sigma-Aldrich and used without purification. Compounds **8**[12] and **10**[13] were synthesized according to literature. Compounds **2**, **3**, **4a**, **4b**, **5a**, **5b**, **6**, **7**, **9** and **P1** were synthesized as described in the following synthetic procedures.

**Scheme 2. Synthesis of (a) TAC Core and (b) the TAC-Containing Small Molecule and Polymer**

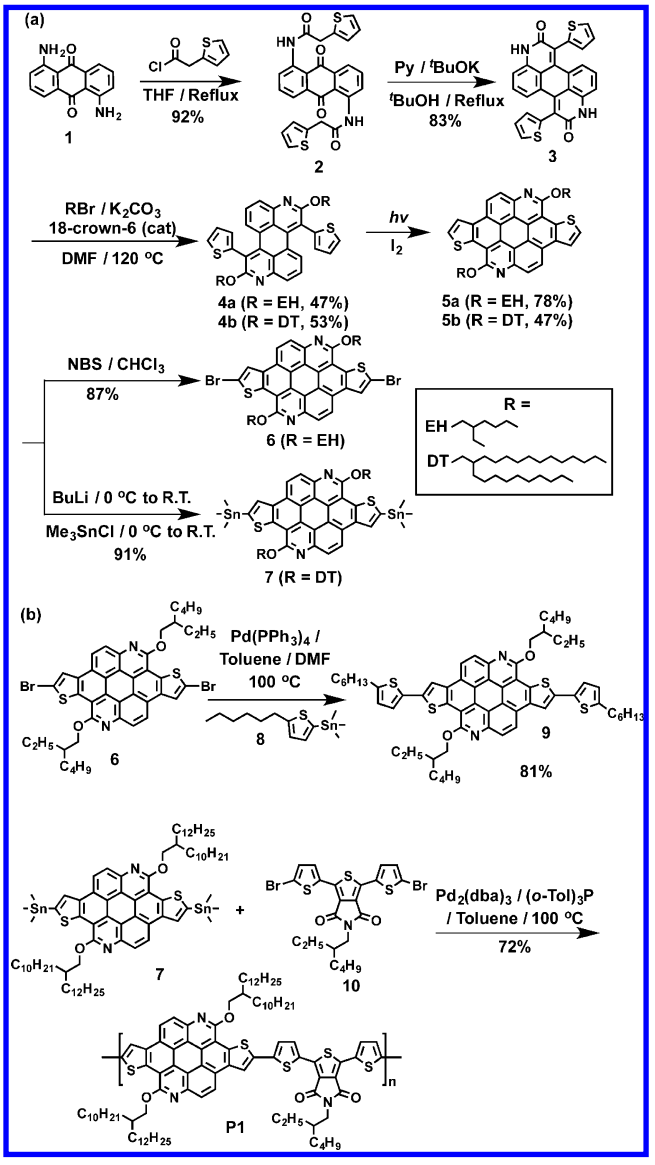


*Compound* ***2***. To a stirring solution of 1,5-diaminoanthraquinone (**1**, 7.00 g, 29.4 mmol, 1.0 equiv) in anhydrous THF (100 mL) was added dropwise 2-thiopheneacetyl chloride (9.91 g, 61.7 mmol, 2.1 equiv) under a $N_2$ atmosphere. After overnight stirring, the resulting suspension was filtered and washed with methanol. The crude product collected from filtration and was further purified by recrystallization from toluene. The title compound (13.1 g, 92%) was obtained as yellow crystals. $^1$H NMR (DMSO-$d_6$, 500 MHz): $\delta$ = 12.06 (s, 2H), 8.94 (dd, $J$ = 7.4 Hz, 2.4 Hz, 2H), 7.89−7.94 (m, 4H), 7.49 (dd, $J$ = 5.1 Hz, 1.0 Hz, 2H), 7.16 (dd, $J$ = 3.4 Hz, 1.1 Hz, 2H), 7.08 (dd, $J$ = 5.1 Hz, 3.4 Hz, 2H), 4.16 (d, $J$ = 0.35 Hz, 4H). $^{13}$C NMR (DMSO-$d_6$, 125 MHz): $\delta$ = 185.75, 169.73, 152.26, 140.77, 135.91, 135.59, 134.52, 127.73, 127.19, 125.98, 125.43, 122.26, 117.48. MS (MALDI-TOF) for $C_{26}H_{18}N_2O_4S_2$: 509.32 $[M + Na]^+$.

*Compound* ***3***. A mixture of **2** (5.00 g, 10.3 mmol, 1.0 equiv), *tert*-BuOK (4.61 g, 41.1 mmol, 4.0 equiv), pyridine (9.75 g, 9.93 mL, 123.3 mmol, 12 equiv) and *tert*-BuOH (80 mL) was refluxed for 24 h under a $N_2$ atmosphere. After the reaction was quenched with water, diluted HCl(aq) (1 M) was added to tune the pH to 7. The resulting precipitate was collected by filtration and washed with bulk water and acetone. The crude product was suspended in hot THF and stirred under reflux for 30 min. After the solution was cooled down and filtered, the title compound **2** was obtained as a deep red solid (3.84 g, 83%). $^1$H NMR (DMSO-$d_6$, 500 MHz): $\delta$ = 12.09 (s, 2H), 7.74 (dd, $J$ = 5.1 Hz, 2H), 7.25 (dd, $J$ = 8.0 Hz, 2H), 7.21 (t, $J$ = 7.9 Hz, 2H), 7.16 (dd, $J$ = 3.5 Hz, 1.2 Hz, 2H), 7.08−7.11 (m, 4H). The acquisition of a $^{13}$C NMR spectrum with a good signal-to-noise ratio was unsatisfactory due to limited solubility. MS (MALDI-TOF) for $C_{26}H_{14}N_2O_2S_2$: 473.26 $[M + Na]^+$.

*Compound* ***4a***. A mixture of **3** (2.70 g, 5.99 mmol, 1.0 equiv), $K_2CO_3$ (2.48 g, 18.0 mmol, 3.0 equiv), 18-crown-6 (catalytic amount) and 2-ethylhexyl bromide (3.47 g, 3.20 mL, 18.0 mmol, 3.0 equiv) in DMF (40 mL) was heated overnight at 120 °C under $N_2$ protection. After the solution cooled down, the excess $K_2CO_3$ was removed by filtration. The filtrate was evaporated to dryness, and the residue was subjected to column chromatography ($SiO_2$, hexanes/$CHCl_3$ 4:1 to 3:1) to yield the title product as semisolid (1.89 g, 47%). $^1$H NMR ($CDCl_3$, 500 MHz): $\delta$ = 7.72 (dd, $J$ = 8.1 Hz, 2.0 Hz, 2H), 7.51 (dd, $J$ = 5.1 Hz, 1.1 Hz, 2H), 7.48 (dd, $J$ = 7.8 Hz, 1.0 Hz, 2H), 7.32 (t, $J$ = 8.0 Hz, 2H), 7.16 (dd, $J$ = 5.1 Hz, 3.5 Hz, 2H), 7.08 (dd, $J$ = 3.5 Hz, 1.1 Hz, 2H), 4.37 (t, $J$ = 4.8 Hz, 4H), 1.69 (m, 2H), 1.29−1.38 (m, 16H), 0.92 (m, 12H). $^{13}$C NMR ($CDCl_3$, 125 MHz): $\delta$ = 161.18, 146.15, 139.28, 138.81, 128.72, 128.69, 128.11, 128.07, 127.74, 127.11, 126.68, 122.93, 115.72, 68.70, 39.09, 30.72, 29.04, 24.13, 23.09, 14.14, 11.26. MS (MALDI-TOF) for $C_{42}H_{46}N_2O_2S_2$: 674.54 $[M]^+$.

*Compound* ***4b***. Synthesis of **4b** was following the same synthetic procedure as **4a**. Yield: 53%. $^1$H NMR ($CDCl_3$, 500 MHz): $\delta$ = 7.73 (dd, $J$ = 8.1 Hz, 1.0 Hz, 2H), 7.51 (dd, $J$ = 5.1 Hz, 1.1 Hz, 2H), 7.48 (dd, $J$ = 7.8 Hz, 1.0 Hz, 2H), 7.31 (t, $J$ = 8.0 Hz, 2H), 7.17 (dd, $J$ = 5.1 Hz, 3.5 Hz, 2H), 7.08 (dd, $J$ = 3.5 Hz, 1.1 Hz, 2H), 4.38 (d, $J$ = 5.3 Hz, 4H), 1.90 (m, 2H), 1.29 (m, 80H), 0.93 (m, 12H). $^{13}$C NMR ($CDCl_3$, 125 MHz): $\delta$ = 161.18, 146.18, 139.28, 138.84, 128.73, 128.67, 128.09, 128.07, 127.74, 127.07, 126.68, 122.93, 115.72, 69.06, 37.57, 34.70, 34.56, 31.98, 31.64, 31.55, 30.17, 30.09, 29.76, 29.72, 29.69, 29.42, 26.84, 25.31, 22.74, 22.70, 20.72, 14.16. MS (MALDI-TOF) for $C_{74}H_{110}N_2O_2S_2$: 1122.76 $[M]^+$.

*Compound* ***5a***. A $CHCl_3$ (100 mL) solution of **4a** (2.00 g, 2.96 mmol) was irradiated with a 300 W incandescent lamp in the presence of iodine for 36 h. The solution was evaporated to give a crude mixture, which was recrystallized from cyclohexane to give the title compound as yellow crystals (1.56 g, 78%). $^1$H NMR ($CDCl_3$, 500 MHz): $\delta$ = 8.47 (d, $J$ = 8.7 Hz, 2H), 8.23 (d, $J$ = 8.6 Hz, 2H), 8.15 (d, $J$ = 5.3 Hz, 2H), 7.93 (d, $J$ = 5.3 Hz, 2H), 4.91 (m, 4H), 2.26 (m, 2H), 2.04 (m, 4H), 1.91 (m, 4H), 1.82 (m, 4H), 1.27 (t, $J$ = 7.5 Hz, 6H), 1.09 (t, $J$ = 7.2 Hz, 6H). $^{13}$C NMR ($CDCl_3$, 125 MHz): $\delta$ = 157.18, 139.37, 135.15, 131.19, 127.93, 126.90, 125.01, 124.2, 123.05, 121.29, 118.11, 114.21, 110.33, 69.60, 39.63, 31.02, 29.49, 24.43, 23.35, 14.37, 11.58. MS (MALDI-TOF) for $C_{42}H_{42}N_2O_2S_2$: 670.48 $[M]^+$.

*Compound* ***5b***. A $CHCl_3$ (100 mL) solution of **4b** (3.50 g, 3.12 mmol) was irradiated with a 300 W incandescent lamp in the presence of iodine for 36 h. The solution was evaporated to give a crude mixture, which was purified by column chromatography ($SiO_2$, hexanes/$CHCl_3$ 2:1) to give the title compound as yellow semisolid (1.64 g, 47%). $^1$H NMR ($CDCl_3$, 500 MHz): $\delta$ = 8.44 (d, $J$ = 8.8 Hz, 2H), 8.23 (d, $J$ = 8.6 Hz, 2H), 8.14 (d, $J$ = 5.5 Hz, 2H), 7.93 (d, $J$ = 5.3 Hz, 2H), 4.93 (d, $J$ = 5.3 Hz, 4H), 2.33 (m, 2H), 2.03 (m, 4H), 1.83 (m, 4H), 1.70 (m, 8H), 1.54 (m, 8H), 1.46 (m, 8H), 1.24−1.37 (m,


dx.doi.org/10.1021/cm5018272 | Chem. Mater. 2014, 26, 3920−3927

46H), 0.85−0.89 (m, 12H). $^{13}$C NMR ($CDCl_3$, 125 MHz): $\delta$ = 157.30, 139.48, 135.22, 131.28, 127.97, 127.01, 125.13, 124.30, 123.12, 121.33, 118.23, 114.34, 110.45, 70.03, 38.19, 31.97, 31.93, 31.88, 30.33, 29.90, 29.86, 29.82, 29.78, 29.71, 29.44, 29.40, 27.26, 22.71, 22.70, 14.12. MS (MALDI-TOF) for $C_{74}H_{106}N_2O_2S_2$: 1119.93 $[M + 1]^+$.

*Compound* **6**. To a $CHCl_3$ (100 mL) solution of **5a** (1.74 g, 2.60 mmol) was added NBS (0.970 g, 5.45 mmol, 2.1 equiv). The mixture was stirred overnight, after which water was added to quench the reaction. The suspension was filtrated and washed with bulk water, acetone and $CHCl_3$ to give **6** as a yellow solid (1.87 g, 87%). $^1$H NMR ($CDCl_3$, 500 MHz): $\delta$ = 7.75 (d, 8.5 Hz, 2H), 7.67 (d, $J$ = 8.3 Hz, 2H), 7.64 (s, 2H), 4.71 (d, $J$ = 5.5 Hz, 4H), 2.20 (m, 2H), 1.63−1.95 (m, 8H), 1.30 (t, $J$ = 7.5, 6H), 1.17 (t, $J$ = 7.2 Hz, 6H). The acquisition of a $^{13}$C NMR spectrum with good signal-to-noise ratio was unsatisfactory due to limited solubility. MS (MALDI-TOF) for $C_{42}H_{40}Br_2N_2O_2S_2$: 826.28 $[M]^+$.

*Compound* **7**. In a $N_2$ protected Schlenk flask, **5b** (1.00 g, 0.890 mmol, 1.0 equiv) was dissolved in anhydrous THF (20 mL). A solution of *n*-BuLi in hexanes (1.45 mL, 1.6 M, 2.32 mmol, 2.6 equiv) was added dropwise at 0 °C. After the solution was stirred for 30 min at 0 °C, the reaction was allowed to stir at room temperature for 1 h. The flask was placed into an ice bath again and trimethyltin chloride in hexanes (2.68 mL, 1.0 M, 3.0 equiv) was injected in one portion. The mixture was allowed to react overnight at room temperature. The reaction was treated with water and extracted with hexane. The organic phase was dried with anhydrous $MgSO_4$ and filtrated. The residue from evaporation of the filtrate was precipitated into ice-cooled methanol. Filtration gave the monomer **7** (1.17 g, 91%) as a yellow solid. $^1$H NMR ($CDCl_3$, 500 MHz): $\delta$ = 9.12 (d, $J$ = 8.9 Hz, 2H), 8.75 (d, $J$ = 8.7 Hz, 2H), 8.61 (s, 2H), 5.07 (d, $J$ = 5.5 Hz, 4H), 2.33 (m, 2H), 1.99−2.01 (m, 4H), 1.64−1.78 (m, 12H), 1.23−1.47 (m, 62H), 0.87 (m, 12H), 0.68 (s, 18H). $^{13}$C NMR ($CDCl_3$, 125 MHz): $\delta$ = 157.96, 141.88, 139.91, 136.97, 136.80, 129.25, 127.23, 125.55, 124.60, 123.50, 119.12, 115.32, 110.89, 70.19, 38.35, 31.95, 31.93, 30.42, 29.91, 29.85, 29.80, 29.76, 29.69, 29.42, 29.37, 27.35, 22.69, 14.12, −7.92. MS (MALDI-TOF) for $C_{80}H_{122}N_2O_2S_2Sn_2$: 1446.76 $[M]^+$.

*Compound* **9**. Compounds **6** (150 mg, 0.180 mmol, 1.0 equiv), **8** (138 mg, 0.420 mmol, 2.3 equiv) and $Pd(PPh_3)_4$ (10.0 mg, 0.05 equiv) were loaded into a 50 mL Schlenk tube. Under $N_2$ protection, toluene (6 mL) and DMF (1.5 mL) were injected into the tube. The mixture was heated to 100 °C for 24 h with stirring. The volatiles were removed under reduced pressure to give a residue, which was purified by column chromatography ($SiO_2$: hexanes/$CHCl_3$ 1:1) to give the target compound **9** as an orange waxy solid (147 mg, 81%). $^1$H NMR ($CDCl_3$, 500 MHz): $\delta$ = 8.19 (d, $J$ = 7.9 Hz, 2H), 8.10 (d, $J$ = 7.9 Hz, 2H), 7.82 (s, 2H), 7.21 (s, 2H), 6.81 (s, 2H), 4.88 (s, 4H), 2.96 (t, $J$ = 7.3 Hz, 4H), 2.28 (m, 2H), 2.04 (m, 4H), 1.72−1.86 (m, 16H), 1.47 (brs, 8H), 1.31 (m, 10H), 1.12 (m, 6H), 1.02 (brs, 6H). $^{13}$C NMR ($CDCl_3$, 125 MHz): $\delta$ = 156.34, 145.87, 138.92, 138.63, 135.59, 135.25, 129.52, 126.25, 124.80, 124.01, 122.99, 122.25, 117.19, 115.98, 113.35, 109.27, 69.66, 39.62, 31.78, 31.66, 31.15, 30.45, 29.62, 29.11, 24.34, 23.51, 22.76, 14.49, 14.22, 11.67. MS (MALDI-TOF) for $C_{62}H_{70}N_2O_2S_2$: 1002.59 $[M]^+$.

*Polymer* **P1**. Compounds **7** (200 mg, 0.145 mmol, 1.0 equiv), **10** (85.3 mg, 0.145 mmol, 1.0 equiv), $Pd_2(dba)_3$ (4.0 mg, 0.004 mmol, 0.03 equiv) and P(*o*-tol)$_3$ (5.3 mg, 0.017 mmol, 0.12 equiv) were placed in a flame-dried Schlenk tube with a stir bar and cycled vacuum/nitrogen purging three times. Dry toluene (16 mL) was then added via syringe, and the reaction vessel was placed in a preheated oil bath at 100 °C and allowed to stir overnight. Bromobenzene (0.5 mL) was then added to the reaction vessel, and the reaction was allowed to stir for 3 h. Then, tributylstanyl thiophene (0.5 mL) was added and the reaction was allowed to stir for further 3 h. The reaction mixture was then cooled to room temperature and precipitated by acetone. The crude purple solid was collected by filtration, followed by sequential Soxhlet extractions with acetone, hexanes and chloroform. The chloroform fraction was passed through a silica plug to give **P1** as a purple solid (162 mg, 72%). The polymer does not show proton resonances in $C_2D_2Cl_4$ or $C_6D_4Cl_2$ due to strong aggregation. GPC: $M_n$ = 20.5 kg/mol, $M_w$ = 113.5 kg/mol, PDI = 5.53.

**Measurements and Instruments.** Proton and carbon nuclear magnetic resonance ($^1$H NMR and $^{13}$C NMR) spectra were recorded on a Bruker Avance500 II, using the deuterated solvent as a lock and tetramethylsilane as an internal standard. All chemical shifts are quoted using the $\delta$ scale, and all coupling constants ($J$) are expressed in Hertz (Hz). Matrix-assisted laser desorption ionization (MALDI) mass spectra were measured on a 4800 MALDI TOF/TOF analyzer from Applied Biosystems. Thermal properties were recorded by using thermal gravity analysis (TGA) (Q5000) and TA Q200 differential scanning calorimetry (DSC). Cyclic voltammetry was performed using a 273A potentiostat (Princeton Applied Research), wherein glassy carbon, platinum and a silver wire act as the working electrode, the counter electrode and the pseudoreference electrode, respectively. Samples were prepared in $CHCl_3$ solution with tetrabutylammonium hexafluorophosphate (0.1 M) as the electrolyte at a scan rate of 100 mV s$^{-1}$, using ferrocene/ferrocenium ($Fc/Fc^+$) redox couple as an internal standard. The HOMO levels of compounds are calculated from the difference between the first oxidation potential ($E_{oxi}$) of the compounds and the oxidation potential of ferrocene ($E_{HOMO} = -(4.8 - E)$ eV).[14] The LUMO levels of compounds were calculated based on the electrochemical HOMO levels and the optical band gap. The molecular weights were determined by PSS-WinGPC (PSS) (pump: alliance GPC 2000) GPC equipped with an RI detector using a PLgel MIXED-B column (particle size: 10 mm, dimensions: 0.8 × 30 cm) calibrated against polystyrene standards. A GPC test was carried out at 30 °C with toluene (1.0 mg/mL) as the solvent. UV−vis-NIR spectra were recorded using a Cary 5000 UV−vis-NIR spectrometer. Film thickness measurements were performed using a Dektak 150 surface profiler. The electrical characteristics of the transistors were measured using the Lakeshore Probe Station model CPX-HF and an Aligent 4155C semiconductor parameter analyzer at room temperature under a vacuum ($10^{-3}$ Torr). A Thermal-Oriel 300W solar simulator provided an AM 1.5G solar illumination at 100 mW cm$^{-2}$ for OPV device testing. A Keithley 236 source-measure unit was used to measure current density−voltage ($J$−$V$) curves.

The X-ray beam[15] (Beamline 7.3.3, Advanced Light Source, Lawrence Berkeley National Laboratory) energy was 10 keV ($\lambda$ here is 1.24). All images were exposed using a Pilatus 1 M detector to record the scattering. The angular dependence X-ray absorption spectroscopy (XAS) experiment was performed in Beamline 8.0.1 in Advanced Light Source, Lawrence Berkeley National Laboratory, Berkeley, CA. The total electron yield (TEY) XAS signals were obtained by monitoring the offset sample current. The energy was calibration using features of C K edge XAS of highly ordered pyrolytic graphite (HOPG). The single crystal data was collected and analyzed at Beamline 11.3.1 in Advanced Light Source.

**Device Fabrication.** Transistors were fabricated in the bottom-gate/top-contact configuration on highly doped n-type (100) Si substrates (<0.02 Ω cm) with 300 nm thick thermally grown silicon dioxide as the dielectric layer. The Si substrates (1.6 × 1.4 cm) were successively ultrasonicated in soap water, water, acetone and isopropyl alcohol. Hexamethyldisilazane (HMDS) was deposited by placing the substrates in a closed crystallization dish with an open vial of HMDS for 2 h. The capacitance per unit area of the gate dielectric layer ($SiO_2$, 300 nm) was Ci = 11.5 nF cm$^{-2}$.[16] The solutions were filtered through poly(tetrafluoroethylene) (PTFE, 0.45 $\mu$m) filters prior to film deposition. All the organic thin films were spuncast onto the HMDS modified Si substrates from tetrahydrofuran solutions (3 mg mL$^{-1}$) at a rotation rate of 3000 rpm for 30 s, followed by annealing at certain temperatures as noted. Sample annealing was carried out for 30 min to 1 h, and followed by slow cooling to room temperature over 1 h. The thickness of each film was measured to be around 20−30 nm. Finally, gold source/drain electrodes (50 nm thick) were evaporated on top through a metal mask (9 pixels/chip) with a channel width of 3 mm and length between 100 and 200 $\mu$m. The average mobility was obtained from a minimum of 3−9 pixels from 1 to 3 different chips. Scratching the $SiO_2$ dielectric layer off n-doped Si substrates provided gate electrodes. The thermal annealing was performed on a hotplate in

a glovebox filled with $N_2$. All the FET measurements were performed under a vacuum ($10^{-3}$ Torr) at room temperature.

Conventional geometry OPVs were fabricated using a device architecture of ITO/$MoO_3$/P1:$PC_{71}BM$ Blend/LiF:Al. Indium tin oxide (ITO)-coated glass substrates were cleaned by successive sonication in soap solution, deionized water, acetone and isopropyl alcohol for 15 min at 40 °C and UV ozone cleaned for 10 min. An ∼40 nm thick PEDOT:PSS layer was prepared by spin-casting its aqueous solution onto the cleaned ITO-coated glass substrate at 4000 rpm for 40 s and baked at 140 °C for 20 min before being transferred to a $N_2$ glovebox. **P1** and $PC_{71}BM$ were each dissolved in chloroform at a concentration of 15 mg/mL and were blended together in a 1:1 ratio prior to being spin-coated onto the PEDOT:PSS film at 1000 rpm for 30 s. Subsequently, the LiF (0.7 nm) and Al (100 nm) were thermally evaporated under a high vacuum (∼$4 \times 10^{-6}$ mbar) at rates of 0.2 and 2 Å $s^{-1}$, respectively. The Al electrodes defined the devices with a shadow mask of 0.03 $cm^2$ in area. The power conversion efficiencies are reported as an average of 5 to 6 devices.

Inverted OPVs were fabricated using a device architecture of ITO/ZnO/P1:$PC_{71}BM$ Blend/$MoO_3$/Ag. ITO-coated glass substrates were cleaned by successive sonication in soap solution, deionized water, acetone and isopropyl alcohol for 15 min at 40 °C and UV ozone cleaned for 10 min. A 20 mM dispersion of ZnO nanoparticles in ethanol, synthesized from a reported procedure,[17] was spin-coated onto the glass substrate at 4000 rpm for 40 s and baked at 120 °C for 10 min. The polymer blend was deposited as in the conventional geometry. Subsequently, the $MoO_3$ (8 nm) and Ag (100 nm) were thermally evaporated under a high vacuum (∼$4 \times 10^{-6}$ mbar) at rates of 0.2 and 2 Å $s^{-1}$, respectively. The Ag electrodes defined the devices with a shadow mask of 0.03 $cm^2$ in area. The power conversion efficiencies are reported as an average of 5 to 6 devices.

## RESULTS AND DISCUSSION

The synthesis of TAC derivatives started (Scheme 2a) from acylation of commercially available 1,5-diaminoanthraquinone

**Scheme 3. Proposed Mechanism for Base-Promoted Tautomerization and Alkylation**

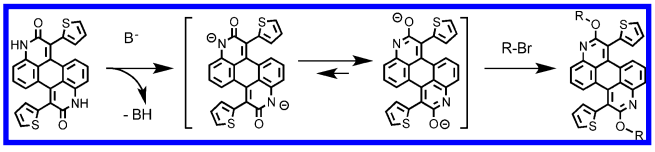


(**1**) to give the diamide **2**, from which the fused **3** was obtained in 83% yield by double intramolecular Knoevenagel condensation. In the following alkylation step, the deprotonation of the amide proton went effectively in the presence of $K_2CO_3$. Thanks to an anion tautomerization (Scheme 3), *O*-alkylation instead of *N*-alkylation occurred to give the aromatized diazaperylene intermediate **4** when 2-ethylhexyl and 2-decyltetradecyl bromides were employed. Compound **4** was prone to undergo thiophene-fusion reactions, and full thiophene annulation was furnished under irradiation in the presence of iodine to give **5a** (EH-TAC) and **5b** (DT-TAC) in 78% and 47% yield, respectively. Further functionalization of TACs was straightforward. Either bromide or trimethyltin were easily introduced to the $\alpha$-position of thiophenes in high yield. Such TAC derivatives are compatible with conventional Stille coupling reaction conditions. As shown in Scheme 2b, small molecule **9** and polymer **P1** were obtained in high yield after coupling **6** and **7** with a thiophene trimethylstannane and a thienopyrrolodione bromide, respectively.

The molecular structure of **5a** was unambiguously confirmed by single crystal X-ray analysis (Figure 1), which also revealed

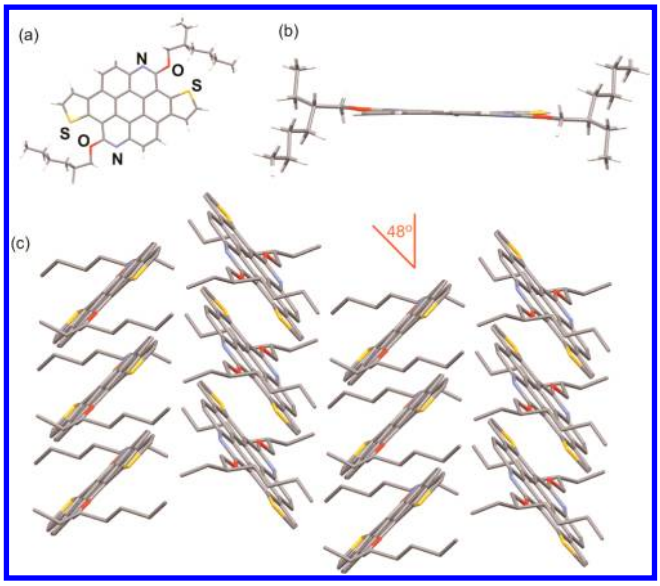


**Figure 1.** Capped stick representation of X-ray structures of EH-TAC. (a) top view, (b) side view and (c) stacked structure showing the slipped herringbone stacking (H atoms were omitted for clarity).

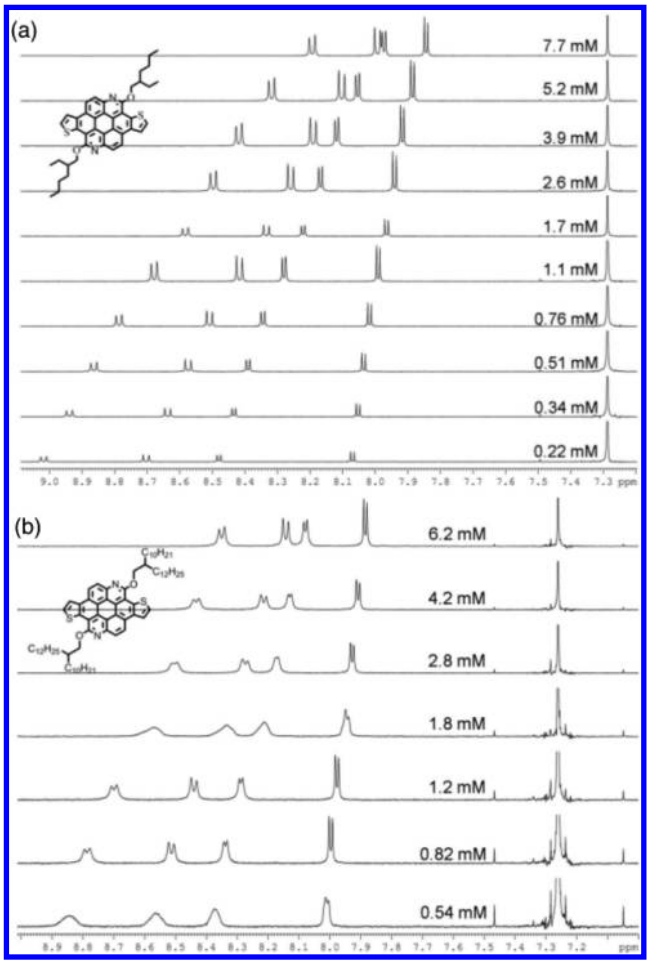


**Figure 2.** $^1H$ NMR spectra ($CDCl_3$, 298 K) of (a) **5a** and (b) **5b** at various concentrations.

the nearly planar conformation of the TAC core. The thiophene units slightly twisted out of the plane of azacoronene with a dihedral angle of only 2.2°. The flat TAC molecules


dx.doi.org/10.1021/cm5018272 | Chem. Mater. 2014, 26, 3920−3927

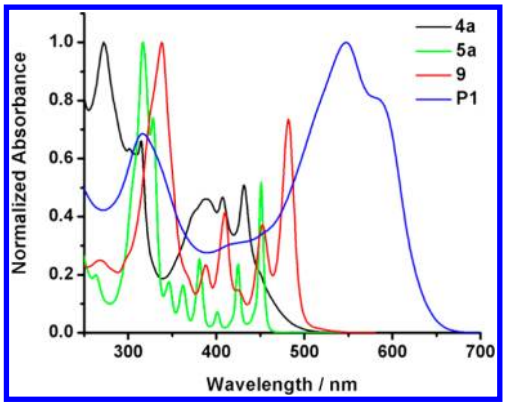


**Figure 3.** UV−vis spectra of **4a**, **5a**, **9** and **P1** in $CHCl_3$.

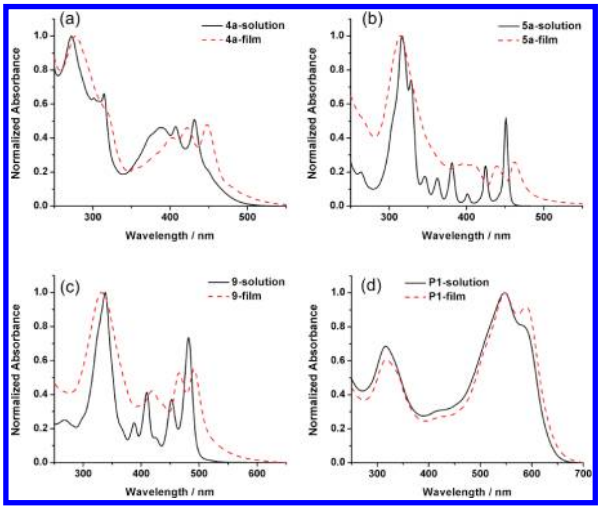


**Figure 4.** Comparison of solution (in $CHCl_3$) and thin film UV−vis spectra of (a) **4a**, (b) **5a**, (c) **9** and (d) **P1**.

**Table 1. List of Optical and Electrochemical Data of TACs in $CHCl_3$ Solution**

| | UV−vis | | | cyclic voltammetry | | |
|---|---|---|---|---|---|---|
| compound | $\lambda_{max}$ [a] (nm) | $\lambda_{onset}$ (nm) | $E_g^{opt}$ (eV) | HOMO (eV) | LUMO (eV) | $E_g^{electro}$ (eV) |
| **4a** | 431 | 491 | 2.52 | n.m.[b] | n.m.[b] | n.m.[b] |
| **4b** | 432 | 491 | 2.52 | n.m.[b] | n.m.[b] | n.m.[b] |
| **5a** | 451 | 460 | 2.69 | −5.42[c] | −2.73[d] | n.o.[e] |
| **5b** | 451 | 459 | 2.70 | −5.42[c] | −2.72[d] | n.o.[e] |
| **9** | 482 | 500 | 2.48 | −5.25[c] | −2.77[d] | n.o.[e] |
| **P1** | 547 | 653 | 1.90 | −5.35[c] | −3.51[c] | 1.84[c] |

[a]The absorption maximum of the peak at the longest wavelength. [b]Not measured. [c]Determined by cyclic voltammetry. [d]Estimated by LUMO = HOMO + $E_g^{opt}$. [e]Not observed.

stacked into a 1D columnar structure along the crystallographic *b*-axis with interplane spacing of 3.34 Å and a centroid-to-centroid distance of 5.02 Å between two adjacent TAC cores, which suggested a slipped $\pi-\pi$ stacking with an angle of 48° between the $\pi$ stacking and the crystallographic *b*-axis. Accordingly, neighboring columns were arranged in a slipped herringbone stacking geometry, with nearly half of TAC's aromatic surface overlapping with the nearby ones.

Aggregation of **5a** and **5b** in $CDCl_3$ solution was revealed by concentration-dependent $^1H$ NMR spectroscopic changes (Figure 2). The absorption spectrum of TAC 5a displayed

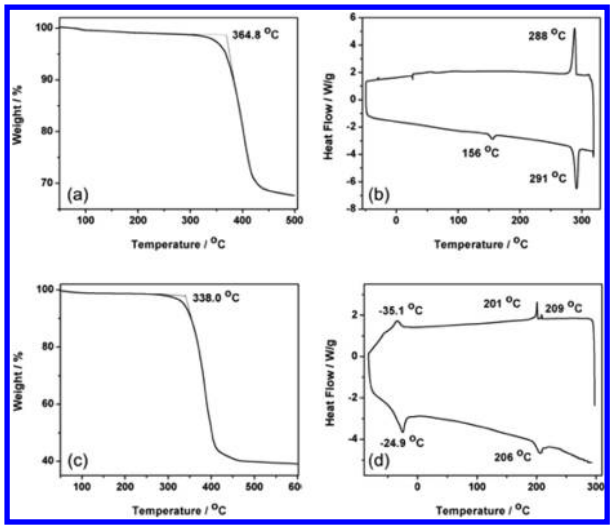


**Figure 5.** Respective TGA (a and c) and DSC curves (b and d) of **5a** (a and b) and **5b** (c and d).

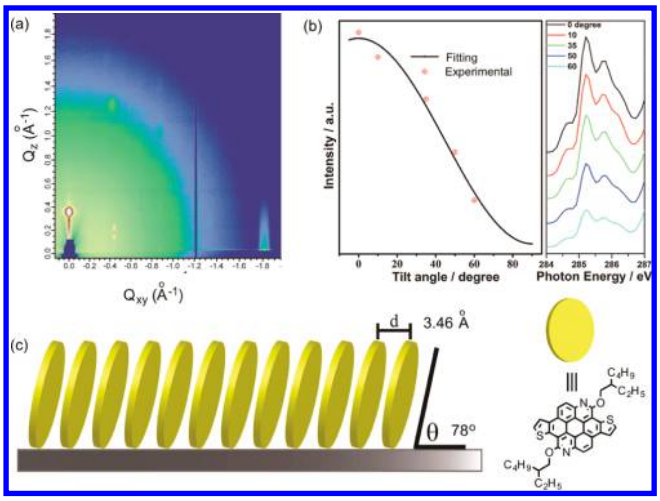


**Figure 6.** (a) GIWAXS pattern and (b) angular dependent NEXAFS of **5a**. (c) Illustration of the molecular organization of **5a** on surface.

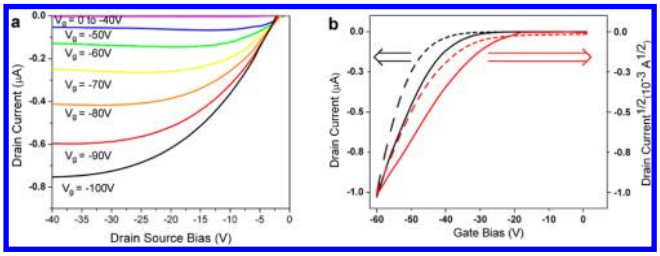


**Figure 7.** Characteristic (a) output curves and (b) transfer curves of annealed spincast films of compound **5a**. In the transfer curves, solid and dashed lines refer to forward and backward voltage scans, respectively.

(Figure 3) six well-resolved absorption bands in the visible region at 451, 425, 402, 381, 363 and 347 nm, together with two overlapping bands at 330 and 318 nm, which were very different from the spectra of the azaperylenes **4a** and **4b**. A linear absorption−concentration relationship, together with the lack of peak shifting in the UV−vis spectra of **5a** within the concentration between 5 and 50 $\mu$M, indicated no aggregation at these low concentrations (Figure S2, Supporting Informa-


dx.doi.org/10.1021/cm5018272 | *Chem. Mater.* 2014, 26, 3920−3927

**Table 2. Summary of Transfer Characteristics of 5a-based OFETs Fabricated at Different Conditions**

| conditions | $\mu_h^{avg,a}$ cm$^2$ V$^{-1}$ s$^{-1}$ | $\mu_h^{dev}$ cm$^2$ V$^{-1}$ s$^{-1}$ | $\mu_h^{max}$ cm$^2$ V$^{-1}$ s$^{-1}$ | $V_{th}$ | $I_{on}/I_{off}$ |
|---|---|---|---|---|---|
| evaporated (as cast) | $4.9 \times 10^{-3}$ | $8.3 \times 10^{-4}$ | $6.0 \times 10^{-3}$ | −13 | $10^3$−$10^4$ |
| evaporated (annealed)[b] | $6.8 \times 10^{-3}$ | $1.8 \times 10^{-3}$ | $8.6 \times 10^{-3}$ | −7 | $10^4$ |
| spincast (as cast) | $2.6 \times 10^{-3}$ | $1.4 \times 10^{-3}$ | $4.0 \times 10^{-3}$ | −17 | $10^3$ |
| spincast (annealed)[b] | $1.3 \times 10^{-2}$ | $5.6 \times 10^{-3}$ | $2.8 \times 10^{-2}$ | −13 | $10^4$ |

[a]The average mobility was obtained from a minimum of 3−9 pixels from 1 to 3 different chips. [b]All films were annealed at 175 °C for 1 h.

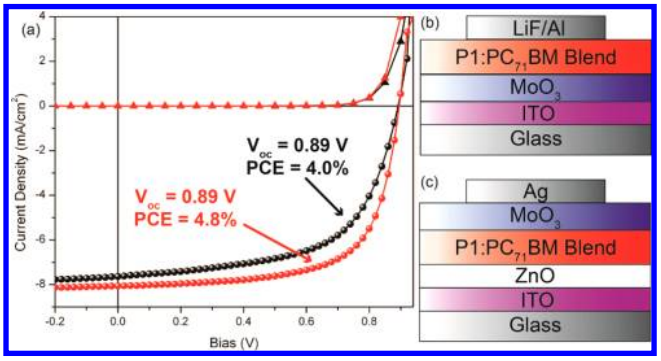


**Figure 8.** (a) $J$−$V$ curves of conventional (black) and inverted (red) OPVs in dark (Δ) or under illumination (·). Illustration of (b) the conventional and (c) the inverted cell architectures.

**Table 3. Device Characteristics of P1-based OPVs[a]**

| cell type | $J_{sc}$ (mA/cm$^2$) | $V_{oc}$ (V) | fill factor | PCE (%) |
|---|---|---|---|---|
| conventional (average)[b] | 6.6 | 0.86 | 0.58 | 3.3 |
| conventional (max) | 7.6 | 0.89 | 0.60 | 4.1 |
| inverted (average)[b] | 7.1 | 0.89 | 0.64 | 4.0 |
| inverted (max) | 8.1 | 0.89 | 0.67 | 4.8 |

[a]Device area is 0.03 cm$^2$ as defined by shadow masks. [b]The PCEs are reported as an average of 5 to 6 devices.

tion). In comparison to **5a**, the attachment of extra thiophenes in **9** led to a red shift of all the peaks. In the spuncast thin film of **5a** and **9** (Figure 4), significant peak broadening as well as bathochromic shifts were observed, indicating molecular aggregation in the solid state. The fine absorption structures associated with TAC disappeared in the solution absorption spectrum of polymer **P1**, instead broad double peaks at 547 and 598 nm were observed. The former band can be attributed to the $\pi$−$\pi^*$ transition and the latter attributable to an intramolecular charge transfer, both being characteristic of donor−acceptor systems.[18] In the thin film, the intensity of the 598 nm peak increased with respect to the 547 nm one (Figure 4d), suggesting stronger interchain packing in the solid state. From the onset of the absorption at the lowest energy, together with electrochemical measurements using cyclic voltammetry (Figure S3, Supporting Information), the optical bandgaps and frontier orbital energies could be estimated (Table 1). Compounds **5a** and **5b** have similar HOMO levels around −5.4 eV, which is significantly lower than those of the reported hexathienocoronoene (−5.08 eV)[10d] and contorted tetrathienocoronenes (−5.10 eV).[10e] Such comparison was based on measurements conducted under similar conditions; however, it should be noted that these optical and electrochemical methods only provide approximations of the real HOMO−LUMO gap.[19] The less electron-rich character of TACs can be explained by fewer fused thiophenes and the presence of two electron withdrawing *N*-heteroatoms. Polymer **P1** also has a low HOMO of −5.35 eV, which as discussed below, is advantageous for high open circuit voltage ($V_{oc}$) in polymer−fullerene based OPVs.[20] The frontier orbitals of methyl-substituted TAC, calculated by density functional theory (DFT) using basis B3LYP/6-31G*, indicates that (Figure S4, Supporting Information) the lowest unoccupied molecular orbital (LUMO) effectively delocalizes on the core. The HOMO contains two nodes on C-6 and C-12 and spreads over both the coronene and thiophene units.

The TACs exhibited excellent thermal stability, as revealed by thermal gravimetric analysis (TGA), whereas differential scanning calorimetry (DSC) analysis indicated side chain dependent metaphase transitions in **5a** and **5b**, with the latter having much lower melting and crystallization temperatures (Figure 5 and S5, Supporting Information). Cooling from the isotropic phase of **5a** resulted in a birefringent mosaic-like texture in polarized optical microscope (POM) images (Figure S6, Supporting Information), which was characteristic for discotic liquid crystalline phase[8b] and also consistent with the columnar stacking in the X-ray structure **5a**.

The TACs showed a high order of supramolecular organization in spuncast thin films, as revealed by GIWAXS measurements (Figure 6a).[21] The meridional reflection in the GIWAXS pattern along $q_z$ at $q_{x,y}$ = 0 is related to an intercolumnar spacing of 1.76 nm. Combined with the in-plane diffraction with a $d$ spacing of 3.46 Å, an edge-on arrangement of **5a** with the column stacking parallel to the substrate can be deduced (Figure 6c). Assuming the same $\pi$−$\pi$ plane separation of 3.34 Å as in the single crystals, the aromatic cores were estimated to tilt ca. 75° with respect to the substrate. This was in great agreement with the angular dependent NEXAFS measurements (Figure 6b), from which a tilt angle of 78° between the aromatic cores and the substrate was obtained (see the Supporting Information for details).

The preferential molecular orientation and high degree of self-organization in **5a** prompted us to investigate its charge transport properties in thin film OFETs. Hexamethyldisilazane (HMDS)-treated silicon substrates were used in the bottom gate, top contact OFET devices, with thin films of **5a** deposited by either evaporation or spin-casting. All OFET devices exhibited *p*-type characteristics (Figure 7). These based on spuncast, thermally annealed films perform better than the thermally deposited ones, with an average and maximum hole mobility of 0.013 cm$^2$ V$^{-1}$ S$^{-1}$ and 0.028 cm$^2$ V$^{-1}$ S$^{-1}$, respectively (Table 2). Although these mobilities are notably lower than those high performing acenes and thienoacenes,[9] they are one order higher than the hexathienocoronenes[10d] and are among the top field effect mobilities for solution processed discotic materials.[20]

As an initial evaluation of the discotic TAC's role as a building block for more versatile electroactive materials, polymer **P1** was tested as the donor material in bulk heterojunction solar cells using both conventional and inverted device geometries (Figure 8). High $V_{oc}$ values of 0.89 V were obtained in both device geometries, accompanied by a fill factor


dx.doi.org/10.1021/cm5018272 | Chem. Mater. 2014, 26, 3920−3927

of up to 0.67 (Table 3). Such a high $V_{oc}$ correlates well with the low HOMO of TAC building block and the resulting **P1** polymer.[21] The conventional OPVs displayed a power conversion efficiency of 4.1%, which was further improved to 4.8% in the inverted device. Despite the less than optimal short circuit current density, it affirms that TAC is a promising electron donor unit, the chemical tunability of which allows for optimization to give new classes of high performance conjugated polymers.

## ■ CONCLUSIONS

In summary, we have reported a concise and regioselective synthesis of the highly versatile thienoazacoronenes, the critical step of which utilizes an anion tautomerization to achieve simultaneous alkylation/aromatization. This synthetic route also provides a convenient pathway to highly functionalized azaperylenes, which is currently under exploration. The incorporation of N and S heteroatoms into a PAH and the alkoxyl substitution effectively modulates the frontier orbital energy levels, which impacts $V_{oc}$ in OPVs. The thiophene-fused core undergoes easy modification at the $\alpha$-position for ready integration into extended conjugated small molecules or polymers. The TACs have shown a remarkable self-organization behavior in various materials states, which allows their incorporation in electronic devices such as OFETs and OPVs. The promising field effect mobilities and high $V_{oc}$ underscore the great potential of TAC as a promising electron donor for the development of high performance organic electronic materials.

## ■ ASSOCIATED CONTENT

### Ⓢ Supporting Information

NEXAFS, CV and POM data. Frontier orbital plots. This material is available free of charge via the Internet at http://pubs.acs.org.

## ■ AUTHOR INFORMATION


### Corresponding Author

*Y. Liu. yliu@lbl.gov.

### Author Contributions

⊥These authors contributed equally.


### Notes

The authors declare no competing financial interest.

## ■ ACKNOWLEDGMENTS

This work was supported by Self-Assembly of Organic/Inorganic Nanocomposite Materials program (B.H. and Y.L.), and was performed at the Molecular Foundry, with the X-ray experiment conducted at Advanced Light Source (ALS), Lawrence Berkeley National Laboratory, all supported by the Office of Science, Office of Basic Energy Sciences, of the U.S. Department of Energy under Contract No. DE-AC02-05CH11231. A.B.P. acknowledges the DOE SULI internship program. We thank Dr. Chenhui Zhu and Dr. Alexander Hexemer at ALS for help with GIWAXS measurements.

## ■ REFERENCES


(1) (a) Hoeben, F. J. M.; Jonkheijm, P.; Meijer, E. W.; Schenning, A. P. H. J. *Chem. Rev.* **2005**, *105*, 1491−1546. (b) Facchetti, A. *Nat. Mater.* **2013**, *12*, 598−600.

(2) (a) Wang, C.; Dong, H.; Hu, W.; Liu, Y.; Zhu, D. *Chem. Rev.* **2011**, *112*, 2208−2267. (b) Dong, H.; Fu, X.; Liu, J.; Wang, Z.; Hu, W. *Adv. Mater.* **2013**, *25*, 6158−6183. (c) Mei, J.; Diao, Y.; Appleton, A. L.; Fang, L.; Bao, Z. *J. Am. Chem. Soc.* **2013**, *135*, 6724−6746.

(3) (a) Brédas, J.-L.; Norton, J. E.; Cornil, J.; Coropceanu, V. *Acc. Chem. Res.* **2009**, *42*, 1691−1699. (b) Cheng, Y.-J.; Yang, S.-H.; Hsu, C.-S. *Chem. Rev.* **2009**, *109*, 5868−5923. (c) Peet, J.; Heeger, A. J.; Bazan, G. C. *Acc. Chem. Res.* **2009**, *42*, 1700−1708. (d) Facchetti, A. *Chem. Mater.* **2010**, *23*, 733−758.

(4) (a) Wu, J.; Pisula, W.; Müllen, K. *Chem. Rev.* **2007**, *107*, 718−747. (b) Pisula, W.; Feng, X.; Müllen, K. *Adv. Mater.* **2010**, *22*, 3634−3649. (c) Xiao, J.; Duong, H. M.; Liu, Y.; Shi, W.; Ji, L.; Li, G.; Li, S.; Liu, X.-W.; Ma, J.; Wudl, F.; Zhang, Q. *Angew. Chem., Int. Ed.* **2012**, *51*, 6094−6098.

(5) (a) Draper, S. M.; Gregg, D. J.; Madathil, R. *J. Am. Chem. Soc.* **2002**, *124*, 3486−3487. (b) Takase, M.; Enkelmann, V.; Sebastiani, D.; Baumgarten, M.; Müllen, K. *Angew. Chem., Int. Ed.* **2007**, *46*, 5524−5527. (c) Bunz, U. H. F. *Chem.—Eur. J.* **2009**, *15*, 6780−6789. (d) Zhao, B.; Liu, B.; Png, R. Q.; Zhang, K.; Lim, K. A.; Luo, J.; Shao, J.; Ho, P. K. H.; Chi, C.; Wu, J. *Chem. Mater.* **2009**, *22*, 435−449. (e) Matena, M.; Stöhr, M.; Riehm, T.; Björk, J.; Martens, S.; Dyer, M. S.; Persson, M.; Lobo-Checa, J.; Müller, K.; Enache, M.; Wadepohl, H.; Zegenhagen, J.; Jung, T. A.; Gade, L. H. *Chem.—Eur. J.* **2010**, *16*, 2079−2091. (f) Takase, M.; Narita, T.; Fujita, W.; Asano, M. S.; Nishinaga, T.; Benten, H.; Yoza, K.; Müllen, K. *J. Am. Chem. Soc.* **2013**, *135*, 8031−8040.

(6) (a) Chernichenko, K. Y.; Sumerin, V. V.; Shpanchenko, R. V.; Balenkova, E. S.; Nenajdenko, V. G. *Angew. Chem., Int. Ed.* **2006**, *45*, 7367−7370. (b) Sun, Y.; Tan, L.; Jiang, S.; Qian, H.; Wang, Z.; Yan, D.; Di, C.; Wang, Y.; Wu, W.; Yu, G.; Yan, S.; Wang, C.; Hu, W.; Liu, Y.; Zhu, D. *J. Am. Chem. Soc.* **2007**, *129*, 1882−1883. (c) Jiang, W.; Zhou, Y.; Geng, H.; Jiang, S.; Yan, S.; Hu, W.; Wang, Z.; Shuai, Z.; Pei, J. *J. Am. Chem. Soc.* **2010**, *133*, 1−3. (d) Nielsen, C. B.; Fraser, J. M.; Schroeder, B. C.; Du, J.; White, A. J. P.; Zhang, W.; McCulloch, I. *Org. Lett.* **2011**, *13*, 2414−2417. (e) Zöphel, L.; Enkelmann, V.; Rieger, R.; Müllen, K. *Org. Lett.* **2011**, *13*, 4506−4509. (f) Xiao, Q.; Sakurai, T.; Fukino, T.; Akaike, K.; Honsho, Y.; Saeki, A.; Seki, S.; Kato, K.; Takata, M.; Aida, T. *J. Am. Chem. Soc.* **2013**, *135*, 18268−18271.

(7) (a) Wu, D.; Zhi, L.; Bodwell, G. J.; Cui, G.; Tsao, N.; Müllen, K. *Angew. Chem., Int. Ed.* **2007**, *46*, 5417−5420. (b) Wu, D.; Pisula, W.; Haberecht, M. C.; Feng, X.; Müllen, K. *Org. Lett.* **2009**, *11*, 5686−5689. (c) Gu, P.-Y.; Zhou, F.; Gao, J.; Li, G.; Wang, C.; Xu, Q.-F.; Zhang, Q.; Lu, J.-M. *J. Am. Chem. Soc.* **2013**, *135*, 14086−14089.

(8) (a) Schmidt-Mende, L.; Fechtenkötter, A.; Müllen, K.; Moons, E.; Friend, R. H.; MacKenzie, J. D. *Science* **2001**, *293*, 1119−1122. (b) Laschat, S.; Baro, A.; Steinke, N.; Giesselmann, F.; Hägele, C.; Scalia, G.; Judele, R.; Kapatsina, E.; Sauer, S.; Schreivogel, A.; Tosoni, M. *Angew. Chem., Int. Ed.* **2007**, *46*, 4832−4887. (c) Wong, W. W. H.; Singh, T. B.; Vak, D.; Pisula, W.; Yan, C.; Feng, X.; Williams, E. L.; Chan, K. L.; Mao, Q.; Jones, D. J.; Ma, C.-Q.; Müllen, K.; Bäuerle, P.; Holmes, A. B. *Adv. Funct. Mater.* **2010**, *20*, 927−938.

(9) (a) Niimi, K.; Shinamura, S.; Osaka, I.; Miyazaki, E.; Takimiya, K. *J. Am. Chem. Soc.* **2011**, *133*, 8732−8739. (b) Sokolov, A. N.; Atahan-Evrenk, S.; Mondal, R.; Akkerman, H. B.; Sánchez-Carrera, R. S.; Granados-Focil, S.; Schrier, J.; Mannsfeld, S. C. B.; Zoombelt, A. P.; Bao, Z.; Aspuru-Guzik, A. *Nat. Commun.* **2011**, *2*, 437. (c) Mori, T.; Nishimura, T.; Yamamoto, T.; Doi, I.; Miyazaki, E.; Osaka, I.; Takimiya, K. *J. Am. Chem. Soc.* **2013**, *135*, 13900−13913.

(10) (a) Li, Z.; Zhi, L.; Lucas, N. T.; Wang, Z. *Tetrahedron* **2009**, *65*, 3417−3424. (b) Gorodetsky, A. A.; Chiu, C.-Y.; Schiros, T.; Palma, M.; Cox, M.; Jia, Z.; Sattler, W.; Kymissis, I.; Steigerwald, M.; Nuckolls, C. *Angew. Chem., Int. Ed.* **2010**, *49*, 7909−7912. (c) Chiu, C.-Y.; Kim, B.; Gorodetsky, A. A.; Sattler, W.; Wei, S.; Sattler, A.; Steigerwald, M.; Nuckolls, C. *Chem. Sci.* **2011**, *2*, 1480−1486. (d) Chen, L.; Puniredd, S. R.; Tan, Y.-Z.; Baumgarten, M.; Zschieschang, U.; Enkelmann, V.; Pisula, W.; Feng, X.; Klauk, H.; Müllen, K. *J. Am. Chem. Soc.* **2012**, *134*, 17869−17872. (e) Kang, S. J.; Kim, J. B.; Chiu, C.-Y.; Ahn, S.; Schiros, T.; Lee, S. S.; Yager, K. G.; Toney, M. F.; Loo, Y.-L.; Nuckolls, C. *Angew. Chem., Int. Ed.* **2012**, *51*, 8594−8597. (f) Chen, L.; Mali, K. S.; Puniredd, S. R.; Baumgarten, M.;

Parvez, K.; Pisula, W.; De Feyter, S.; Müllen, K. *J. Am. Chem. Soc.* **2013**, *135*, 13531−13537.
(11) (a) Li, Y.; Xu, W.; Di Motta, S.; Negri, F.; Zhu, D.; Wang, Z. *Chem. Commun.* **2012**, *48*, 8204−8206. (b) Usta, H.; Newman, C.; Chen, Z.; Facchetti, A. *Adv. Mater.* **2012**, *24*, 3678−3684. S3678/3671-S3678/3677. (c) Zhou, W.; Jin, F.; Huang, X.; Duan, X.-M.; Zhan, X. *Macromolecules* **2012**, *45*, 7823−7828. (d) Zhou, W.; Zhang, Z.-G.; Ma, L.; Li, Y.; Zhan, X. *Sol. Energy Mater. Sol. Cells* **2013**, *112*, 13−19.
(12) Pan, Z.; Liu, Y.; Fan, F.; Chen, Y.; Li, Y.; Zhan, X.; Song, Y. *Chem.—Eur. J.* **2013**, *19*, 9771−9774.
(13) (a) Umeyama, T.; Oodoi, M.; Yoshikawa, O.; Sagawa, T.; Yoshikawa, S.; Evgenia, D.; Tezuka, N.; Matano, Y.; Stranius, K.; Tkachencko, N. V.; Lemmetyinen, H.; Imahori, H. *J. Mater. Chem.* **2011**, *21*, 12454−12461. (b) Zhou, E.; Cong, J.; Tajima, K.; Yang, C.; Hashimoto, K. *J. Phys. Chem. C* **2011**, *116*, 2608−2614.
(14) Pommerehne, J.; Vestweber, H.; Guss, W.; Mahrt, R. F.; Bässler, H.; Porsch, M.; Daub, J. *Adv. Mater.* **1995**, *7*, 551−554.
(15) Hexemer, A.; Bras, W.; Glossinger, J.; Schaible, E.; Gann, E.; Kirian, R.; MacDowell, A.; Church, M.; Rude, B.; Padmore, H. *J. Phys.: Conf. Ser.* **2010**, *247*, 012007.
(16) Zhang, Y.; Hanifi, D.; Alvarez, S.; Antonio, F.; Pun, A.; Klivansky, L. M.; Hexemer, A.; Ma, B.; Liu, Y. *Org. Lett.* **2011**, *13*, 6528−6531.
(17) Tan, M. J.; Zhong, S.; Li, J.; Chen, Z.; Chen, W. *ACS Appl. Mater. Interfaces* **2013**, *5*, 4696−4701.
(18) Stalder, R.; Mei, J. G.; Reynolds, J. R. *Macromolecules* **2010**, *43*, 8348−8352.
(19) Bredas, J.-L. *Mater. Horiz.* **2014**, *1*, 17−19.
(20) O'Neill, M.; Kelly, S. M. *Adv. Mater.* **2011**, *23*, 566−584.
(21) Li, Y. *Acc. Chem. Res.* **2012**, *45*, 723−733.